LETTER

NJC
www.rsc.org/njc

Formation of cyano-bridged molecule-based magnetic nanoparticles within hybrid mesoporous silica†

Guylhaine Clavel, Yannick Guari,* Joulia Larionova* and Christian Guérin

Laboratoire de Chimie Moléculaire et Organisation du Solide (LCMOS; CNRS UMR 5637), Université Montpellier II, Place E. Bataillon, 34095 Montpellier cedex 5, France. E-mail: joulia@univ-montp2.fr, guari@univ-montp2.fr.; Fax: +33 4 67 14 38 52

Received (in Montpellier, France) 9th August 2004, Accepted 10th November 2004
First published as an Advance Article on the web 17th January 2005

A new approach for the synthesis and organization of cyano-bridged molecule-based magnetic nanoparticles has been developed using a mesostructured hybrid silica containing $-(CH_2)_2C_5H_4N$ groups as matrix.

The development of nanometer-scaled magnetic particles has attracted much attention in modern science because of their technological and fundamental scientific importance.[1] These materials often exhibit new interesting size-dependent physical and chemical properties, which cannot be achieved by their bulk counterparts, and they could find applications in many fields, including magnetic storage devices, ferrofluids, magnetic refrigeration systems, magnetic carriers for drug targeting and others.[2] A general route to the synthesis of magnetic nanoparticles consists in the use of different surfactants along with organic and mineral matrices, which often provide not only the stabilization of nanoparticles and avoid their aggregation but also offer size control and organization in space. In this respect, the synthesis and structuring of various nanocomposite materials containing nanoscale magnetic particles based on metals or metal oxides have been reported.[3]

In recent years, extensive interest has been dedicated to nanocomposites containing nano-sized molecule-based magnetic materials, such as clusters presenting single-molecule magnetic behaviour[4] or nano-sized molecule-based magnets.[5] The synthesis, structuring and investigation of their unexpected chemical and physical properties has emerged as a promising subject for future developments in nanomaterial science.

The numerous bimetallic assemblies with Prussian Blue like structure based on cyanometallate building blocks form an important family of molecule-based magnetic materials presenting high critical temperatures and interesting physical properties, such as photoinduced magnetism. The variety of structures, magnetic, optical and photomagnetic properties in this family of compounds has been extensively investigated for bulk materials.[6] Mann and co-workers were the first to perform a spatial confinement in the growth of Prussian Blue nanoparticles using the reverse micelles technique.[7] More recently, the syntheses of nano-sized Prussian Blue analogues have also been reported using polymer,[8] inorganic[9] or biomolecular templates.[10] However, to the best of our knowledge, mesostructured silica hosts have never been used in order to grow and organize nanoparticles of molecule-based magnets.

Here, we report a new approach for the growth and structuring of nanoparticles of cyano-bridged molecule-based magnets using mesostructured hybrid silica as a nanoreactor. As depicted in Scheme 1, our strategy consists in the intrapore growth of cyano-bridged networks at specific sites of the hybrid silica, performed by consecutive (step-by-step) coordination of M^{n+} (Fe^{2+}, Ni^{2+}, Fe^{3+}) and $[M'(CN)_m]^{3-}$ [M′ = Fe^{3+} (m = 6), Mo^{5+} (m = 8)]. A mesostructured silica containing $-(CH_2)_2C_5H_4N$ functionalities not only allows growth control but also provides chemical anchoring for the molecule-based magnetic nanoparticles into the silica pores.

A mesostructured hybrid silica SBA-15 with a pore diameter of 75 Å was synthesized using a triblock (P123) copolymer as surfactant.[11] The grafting of the organic functionality $-(CH_2)_2C_5H_4N$ into the silica pores was achieved by using the organometallic compound $(CH_3O)_3Si(CH_2)_2C_5H_4N$.[12] The resulting hybrid silica, of formula $NC_5H_4(CH_2)_2SiO_{1.5}\cdot 11SiO_2$ as inferred from elemental analysis, was used for the intrapore growth and chemical anchoring of nano-sized molecule-based magnets. Silica-based nanocomposite materials containing $Fe^{2+}/[Fe(CN)_6]^{3-}$ (**1**), $Ni^{2+}/[Fe(CN)_6]^{3-}$ (**2**), $Fe^{3+}/[Mo(CN)_8]^{3-}$ (**3**) and $Ni^{2+}/[Mo(CN)_6]^{3-}$ (**4**) were synthesized as follows: the silica powder was successively treated with a methanolic solution of M^{n+} (Fe^{2+} for **1**, Ni^{2+} for **2** and **4**; Fe^{3+} for **3**) and a methanolic solution of $[N(C_4H_9)_4]_3[M'(CN)_m]$[13,14] [M′ = Fe for **1** and **2** (m = 6) and Mo for **3** and **4** (m = 8)]. At each step of the treatment, the silica powder was thoroughly washed with methanol and dried *in vacuo*. Subsequently, this silica powder double treatment

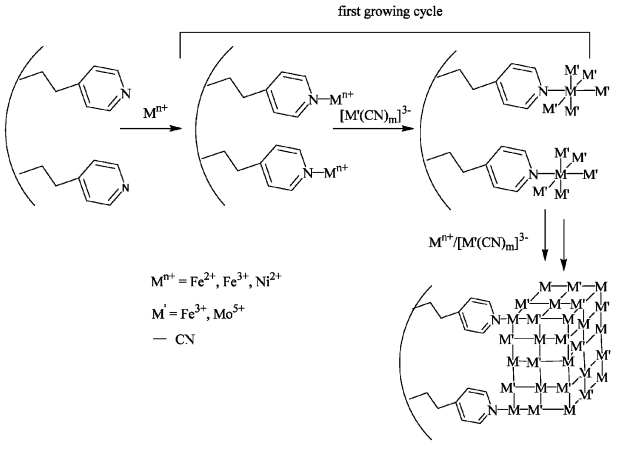

Scheme 1 Schematic representation of the intrapore growth of cyano-bridged molecule-based magnetic nanoparticles.

† Electronic supplementary information (ESI) available: elemental analysis results for compounds **1–4**; UV-Vis spectra of $Fe_4[Fe(CN)_6]_3$ and **1**; IR spectra of reference materials and title compounds **1–4**; powder X-ray diffraction patterns of pristine functionalized and non-functionalized silicas **2** and **3**; plot of the Fe and Ni atomic content *versus* number of impregnation cycles; nanoparticle size distribution diagram. See http://www.rsc.org/suppdata/nj/b4/b412315h/

DOI: 10.1039/b412315h

Table 1 Elemental analysis, IR, Raman and UV-Vis spectroscopic data of nanocomposites **1–4** and corresponding bulk molecule-based magnets

Samples	Growth cycle pair $M^{n+}/[M'(CN)_m]^{3-}$ or bulk material	M : M′ : Si atomic ratio	IR ν(CN)/cm^{-1}	Raman/cm^{-1}	UV-Vis λ/nm
1	$Fe^{2+}/[Fe(CN)_6]^{3-}$	10.6 : n.a. : 89.4	2080 (s)	2150	667
$Fe_4[Fe(CN)_6]_3$	Bulk material	100 : n.a. : n.a.	2078 (s)	2150	654
2	$Ni^{2+}/[Fe(CN)_6]^{3-}$	4.0 : 3.2 : 92.8	2099 (s), 2163 (w)	2185	410
$Ni_3[Fe(CN)_6]_2$	Bulk material	60 : 40 : n.a.	2097 (s), 2166 (w)	2185	400
3	$Fe^{3+}/[Mo(CN)_8]^{3-}$	14.4 : 4.3 : 81.3	2122 (s)	—[a]	825
$Fe[Mo(CN)_8]$	Bulk material	50 : 50 : n.a.	2136 (s)	—[a]	820
4[b]	$Ni^{2+}/[Mo(CN)_8]^{3-}$	5.5 : 3.5 : 91	2152 (s)	2177	610

[a] No peaks corresponding to the stretching vibrations of the cyano groups could be observed. [b] No bulk molecule-based magnet related to **4** could be obtained.[15]

with $M^{n+}/[M'(CN)_m]^{3-}$ will be regarded as one growth cycle. Three consecutive growth cycles were performed on each sample, after which the incorporation procedure did not increase the amount of inserted materials. It is noteworthy that all the pyridine groups $-(CH_2)_2C_5H_4N$ in the silica were coordinated by M^{n+} after the first growth cycle as shown by elemental analysis (see Electronic supplementary information, ESI). The atomic ratio M : M′ : Si for nanocomposite materials **1–4**, given by energy dispersive X-ray analysis (EDAX), and confirmed by elemental analysis, is given in Table 1. It is important to note that, when a non-functionalized silica with a pore size of 75 Å was used for the intrapore growth of molecule-based magnetic nanoparticles in place of the hybrid silica, no incorporation was detected.

While the first growth cycle is performed, the silica powder acquires the colour of the corresponding bulk magnet: blue for **1**, yellow for **2**, green-blue for **3** and green for **4**. The colour intensity of these materials increases with the number of growth cycles. Electronic spectra in the UV-Vis region performed on samples **1–4** show adsorption bands corresponding to inter-metal charge-transfer bands from M to M′ of the related bulk compounds (Table 1 and Fig. 1S, see ESI). The IR and Raman spectra of nanocomposites **1–4** clearly show the bands and peaks corresponding to the stretching vibrations of the bridging cyano groups,[16] which can also be found in the spectra of the respective bulk cyano-bridged molecule-based magnets (Table 1). The IR spectra of the nanocomposites also present SiO_2 vibration bands at 1080, 948, 798 and 459 cm^{-1} (Fig. 2S, see ESI).

In order to determine the effect of the insertion on the structure and porosity of the host matrix, the inserted materials **1–4** were studied by nitrogen physisorption and X-ray diffraction (XRD) analysis. The nitrogen physisorption isotherms and pore-size distribution of the hybrid silica before and after incorporation of $Fe^{2+}/[Fe(CN)_6]^{3+}$ at the first and third cycles (nanocomposite **1**) are shown in Fig. 1. The pristine silica shows a typical adsorption/desorption isotherm of type IV with an H1 hysteresis loop. No change in the isotherm type is observed after intrapore growth of the Prussian Blue phase, proving that the cylindrical pore system is conserved. The amount of adsorbed nitrogen and the BET (Brunauer–Emmett–Teller) surface are reduced with increasing pore filling, that is, the number of growth cycles. However, mesoporosity can still be found, which again proves the preservation of the mesoporous host structure and leads to the conclusion that the particles form inside the pores. The mean pore diameter decreases accordingly, as indicated by the shift of the peak of the pore-size distribution to smaller value (Insert in Fig. 1). All these results clearly demonstrate a progressive filling of the pores by the guest species. The total pore volume calculated at p/p_0 = 0.9 is 0.98 cm^3 g^{-1} for the pristine hybrid silica and 0.43 cm^3 g^{-1} for the nanocomposites after the third impregnation cycle. This indicates a degree of filling of the pores of over 56%. The observed nitrogen physisorption effects are well-known in the literature for intrapore formation inside different host–guest systems.[17] Selected results from nitrogen physisorption analyses of nanocomposites **1–4** obtained after three growth cycles are gathered in Table 2. In all cases, an important decrease in accessible surface and porosity is observed for the nanocomposites with a degree of filling of the pores of around 50%.

The XRD patterns at 2θ (0–10°) of the mesoporous silica after successive incorporations of $M^{n+}/[M'(CN)_m]^{3-}$ show no changes in the peaks positions compared to the XRD pattern of the pristine silica, clearly indicating that it keeps its hexagonal structure (Table 2). However, a consecutive reduction of the X-ray peak intensities, with respect to the pristine silica, was observed for all nanocomposites (Fig. 3S, see ESI). The intensity of the Bragg reflections originates from the difference of scattering power between the silica walls and the empty pores. Due to the impregnation of the pores with scattering material, the amount of scattering power within the pores is increased, resulting in an overall loss of intensity due to phase cancellation between pore walls and guest species.[18]

The results of the nitrogen physisorption and X-ray diffraction analyses were substantiated by transmission electron microscopy (TEM). The TEM micrographs of the pristine hybrid silica clearly show the hexagonal ordering of the pores [Fig. 2(a)]. The TEM analysis performed on nanocomposites **1–4** indicates that the mesostructure of the parent materials is still retained. A TEM micrograph of nanocomposite **1** is given as an example in Fig. 2(b). No out-of-pore isolated particles were visible. Distinctive signals for M and M′ were detected by

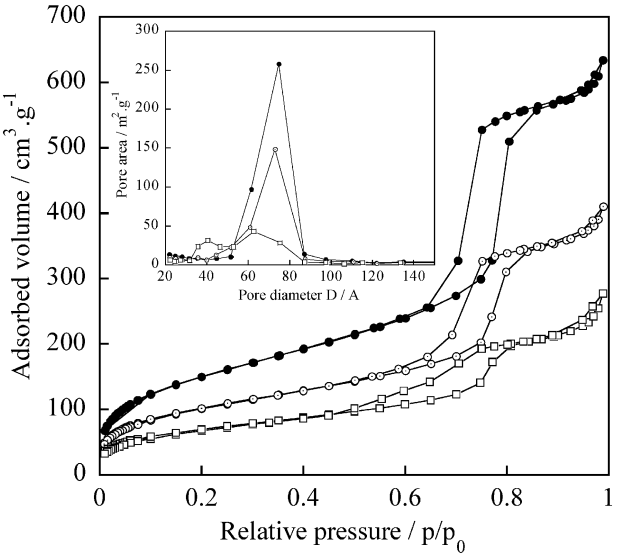

Fig. 1 Nitrogen adsorption/desorption isotherms from the hybrid silica before (●) and after incorporation of $Fe^{2+}/[Fe(CN)_6]^{3-}$ at the first (○) and third (□) growth cycles, for nanocomposite **1**. Insert: Barret–Joyner–Hellenda (BJH) pore-size distribution calculated from the desorption branch of the hybrid silica before (●) and after incorporation of $Fe^{2+}/[Fe(CN)_6]^{3-}$ at the first (○) and third (□) cycles.

Table 2 Relevant physical characteristics of the pristine hybrid mesoporous silica and nanocomposites **1–4**[a]

Sample	$S_{BET}/m^2\ g^{-1}$	$V_p/cm^3\ g^{-1}$	D_p^a/Å	d_{100}/Å	d_{110}/Å	d_{200}/Å
Hybrid silica	542	0.96	75	0.798	1.382	1.596
1	239	0.43	63	0.794	1.365	1.594
2	274	0.51	64	0.808	1.390	1.609
3	195	0.31	64	0.789	1.365	1.581
4	259	0.56	67	0.783	1.360	1.571

[a] Calculated from the desorption branch of the nitrogen sorption isotherm by using the Barret–Joyner–Hellenda (BJH) method.

energy dispersive spectroscopy (EDS) analysis (Fig. 4S, see ESI). The atomic ratio M : M′ : Si, as inferred from elemental analysis, for nanocomposites **1–4** is given in Table 1. As expected, no aggregates could be observed in the pores, which is indicative of a homogeneous dispersion of the cyano-bridged polymer network. Nanoparticles of molecule-based magnets could be clearly seen after removal of silica from the nanocomposite materials with HF. Fig. 2(c) shows a TEM micrograph performed on an extractive replica of nanocomposite **1**. A single distribution with a mean size value of 5 nm could be observed (Fig. 5S, see ESI). This value is slightly smaller than the pore channel mean diameter of 7.5 nm obtained from BET measurements. Obviously, the pore size of the silica matrix precludes further growth of the cyano-bridged network and the aggregation of the so-formed nanoparticles.

Magnetic measurements confirmed the formation of the nanoparticles. Fig. 3 shows the zero-field-cooled (ZFC) and field-cooled (FC) magnetization curves in the range of 2–8 K obtained for the nanocomposite **1**. For the ZFC experiment, the sample was cooled in zero field and then heated in a field of 10 Oe, while the net magnetization of the sample was recorded. The FC data were obtained by cooling the sample under a magnetic field of 10 Oe after the ZFC experiments and recording the change in net sample magnetization with temperature. The ZFC curve shows a narrow peak at 2.25 K, which indicates the blocking temperature (T_B) of the nanoparticles with a mean volume. The critical temperature (T_c) for bulk Prussian Blue is equal to 5.6 K and a T_B around 2.5 K was observed for previously reported Prussian Blue nanoparticles with a size below 12 nm.[8a] The FC curve increases with decreasing temperature and never reaches saturation, indicating that, even at the lowest investigated temperature, a fraction of the particles is still in the superparamagnetic state. The FC and ZFC curves coincide at high temperatures and start to separate at 2.7 K, indicating the blocking temperature of the largest particles. The closeness of T_B to the temperature where the ZFC and FC curves separate indicates the presence of nanoparticles with a narrow size distribution. These results are confirmed by alternating current (AC) susceptibility measurements at five different frequencies in a zero applied direct current (DC) field, which show a frequency-dependent behaviour in the in-phase (χ_m') and the out-of-phase (χ_m'') components (insert in Fig. 3).

In this work, we have developed a new approach for the growth and organization of cyano-bridged molecule-based magnetic nanoparticles using hybrid mesostructured silica as the matrix. We have shown that the hybrid silica host with pyridine functionalities allows intrapore controlled growth of molecule-based nanoparticles and provides covalent anchorage in the pores, leading to a uniform dispersion. This approach opens a new perspective for the preparation of a large range of nano-sized molecule-based magnets.

Experimental

In a typical experiment, modified silica powder (75 mg), prepared from literature procedures, [11, 12] was added to a 10^{-2} M solution of $[Fe(H_2O)_6]Cl_2$ in methanol. The mixture was stirred overnight at room temperature. After filtration, the powder was thoroughly washed several times with methanol and dried at room temperature for 24 h *in vacuo*. The resulting powder was added to a 10^{-2} M methanolic solution of $[N(C_4H_9)_4]_3[Fe(CN)_6]$.[13] The mixture was stirred 48 h, then the powder was filtered, thoroughly washed with methanol and

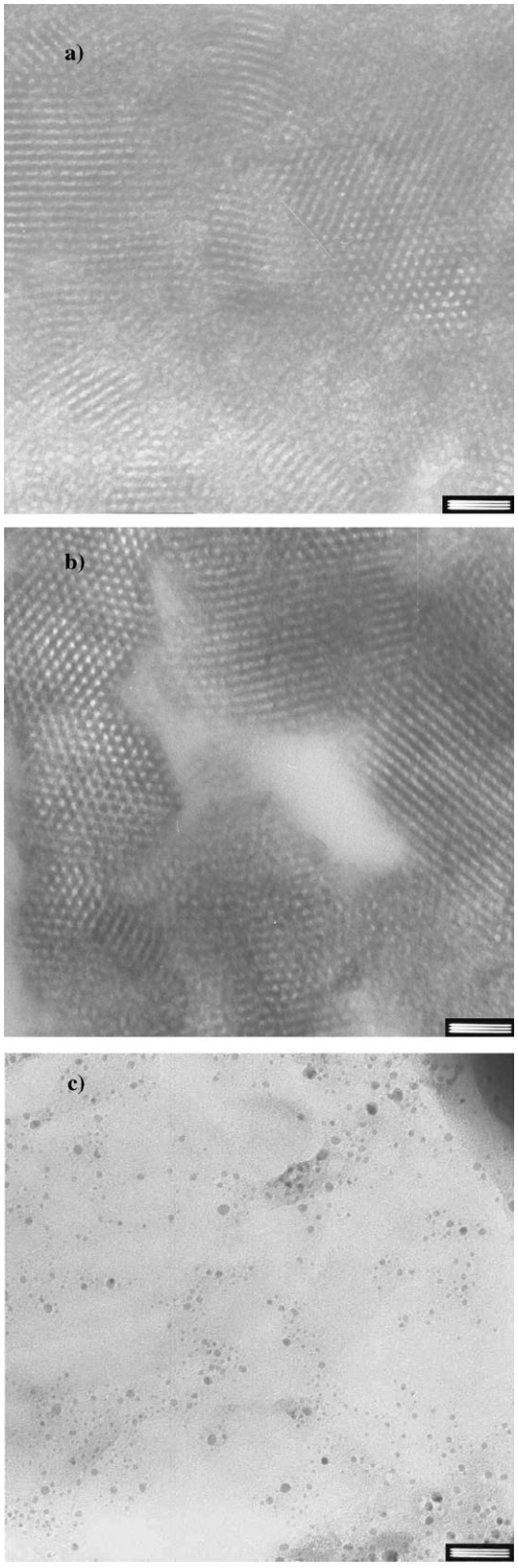

Fig. 2 TEM micrographs of (a) the pristine hybrid silica showing the hexagonal structure; (b) nanocomposite **1**; (c) the nanoparticles obtained from nanocomposite **1** after removal of the silica matrix by HF treatment (extractive replicas). Scale bars = 50 nm.

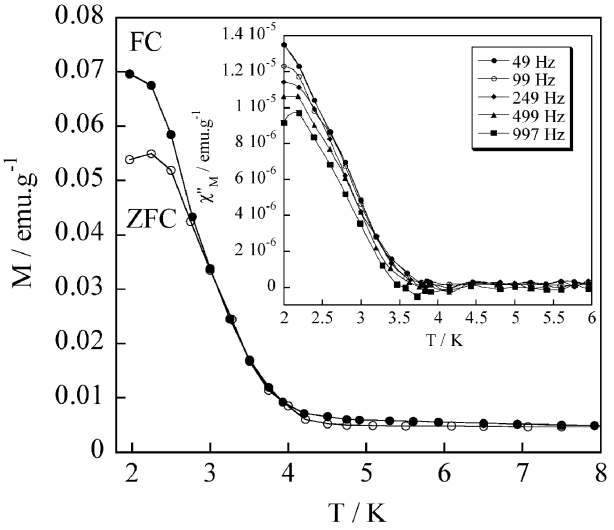

Fig. 3 Zero-field-cooled (ZFC) and field-cooled (FC) magnetization *versus* temperature plots for nanocomposite **1** at an external magnetic field of 10 Oe. Insert: Thermal variation of the out-of-phase susceptibility with zero DC magnetic field at different frequencies of the oscillating magnetic field (3 Oe) for nanocomposite **1**.

dried *in vacuo* to give **1**. This first treatment (or growth cycle) was repeated twice. The complexes used in the two steps for the other inserted materials were: $[Ni(H_2O)_6]Cl_2$, $[N(C_4H_9)_4]_3[Fe(CN)_6]$ for **2**; $[Fe(H_2O)_6]Cl_3$, $[N(C_4H_9)_4]_3[Mo(CN)_8]$[14] for **3**; $[Ni(H_2O)_6]Cl_2$, $[N(C_4H_9)_4]_3[Mo(CN)_8]$ for **4**.

Specific surface areas were determined by the Brunauer–Emmett–Teller (BET) method with a Micromeritics ASAP 2010 analyzer. Elemental analyses were performed by the Service Central d'Analyse (CNRS, Vernaison, France). IR spectra were recorded on a Perkin Elmer 1600 spectrometer with a 4 cm^{-1} resolution. UV-Vis spectra were recorded on KBr disks on a Cary 5E spectrometer. Powder X-ray diffraction patterns were measured on a Bruker D5000 diffractometer equipped with a rotating anode (Institut Européen des Membranes, Montpellier, France). Transmission electron microscopy (TEM) analyses were carried out at 100 kV (JEOL 1200 EXII). Samples for TEM measurements were prepared using ultramichrotomy techniques and deposited on copper grids. Extractive replicas were prepared in order to remove the silica from the samples. Magnetic susceptibility data were collected with a Quantum Design MPMS-XL SQUID magnetometer. The data were corrected for the sample holder and the diamagnetism contributions calculated from the Pascal's constants.[19]

Acknowledgements

The authors thank Dr Arie van der Lee (IEM, UMR 5635, Montpellier, France) for XRD measurements and Mr Alain Mari (LCC, Toulouse, France) for magnetic measurements. The authors also thank the CNRS and the Université Montpellier II for financial support.

References

1 (*a*) T. Hyeon, *Chem. Commun*., 2003, 927; (*b*) K. J. Klabunde, in *Nanoscale Materials in Chemistry*, ed. K. J. Klabunde, Wiley Interscience, New York, 2001; (*c*) M. R Diehl, J.-Y. Yu, J. R. Heath, G. A. Doyle, S. Sun and C. B. Murray, *J. Phys. Chem. B*, 2001, **105**, 7913; (*d*) D. L. Leslie-Pelescky and R. D. Rieke, *Chem. Mater*., 1996, **8**, 1770.

2 (*a*) D. D. Awschalom and D. P. Di Vicenzo, *Phys. Today*, 1995, **4**, 43; (*b*) K. Raj and R. Moskowitz, *J. Magn. Magn. Mater*., 1990, **85**, 233; (*c*) M. L. Billas, A. Chatelain and W. A. de Heer, *Science*, 1994, **265**, 1682; (*d*) R. C. O'Handley, *Modern Magnetic Materials*, Wiley, New York, 1999; (*e*) L. Shen, P. E. Laibinis and T. A. Hatton, *Langmuir*, 1999, **15**, 447; (*f*) R. D. McMichael, R. D. Shull, L. J. Swartzendruber, L. H. Bennet and R. E. Watson, *J. Magn. Magn. Mater*., 1992, **111**, 29; (*g*) B. R. Peters, R. A. Williams and C. Webb, *Magnetic Carrier Technology*, Butterworth-Heinemann, Ltd., Oxford, England, 1992; (*h*) B. M. Berkovsky, V. F. Medvedev and M. S. Krakov, *Magnetic Fluids: Engineering Applications*, Oxford University Press, Oxford, 1993.

3 See, for instance: (*a*) D. P. Dinega and M. G. Bawendi, *Angew. Chem., Int. Ed*., 1999, **38**, 1788; (*b*) V. F. Puntes, K. M. Krishnan and A. P. Alivasatos, *Appl. Phys. Lett*., 2001, **78**, 2178; (*c*) M. Pileni, *Langmuir*, 1997, **11**, 1198; (*d*) F. Dumestre, B. Chaudret, C. Amiens, P. Renaud and P. Fajes, *Science*, 2004, **303**, 821; (*e*) C. B. Murray, S. Sun, W. Gaschler, H. Doyle, T. A. Betley and C. R. Kagan, *IBM J. Res. Dev*., 2001, **45**, 47; (*f*) S. H. Sun and H. Zeng, *J. Am. Chem. Soc*., 2002, **124**, 8204; (*g*) D. Rabelo, E. C. D. Lima, A. C. Reis, W. C. Nunes, M. A. Novak, V. K. Garg, A. C. Oliveira and P. C. Morais, *Nano Lett*., 2001, **1**, 105; (*h*) M. Breulmann, H. Cölfen, H.-P. Hentze, M. Antonietti, D. Walsh and S. Mann, *Adv. Mater*., 1998, **10**, 237; (*i*) V. Matsura, Y. Guari, J. Larionova, C. Guérin, A. Caneschi, C. Sangregorio, E. Lancelle-Beltran, A. Mehdi and R. J. P. Corriu, *J. Mater. Chem*., 2004, **14**, 3026.

4 (*a*) T. Corradin, J. Larionova, A. A. Smith, G. Rogez, R. Clérac, C. Guérin, G. Blondin, R. E. P. Winpenny, C. Sanchez and T. Mallah, *Adv. Mater*., 2002, **14**, 896; (*b*) S. Willemin, G. Arrachart, L. Lecren, J. Larionova, T. Corradin, R. Clérac, T. Mallah and C. Sanchez, *New. J. Chem*., 2003, **27**, 1533; (*c*) B. Folch, J. Larionova, Y. Guari, C. Guérin, A. Mehdi and C. Reyé, *J. Mater. Chem*., 2004, **14**, 2703; (*d*) M. Clemene-Léon, E. Coronado, A. Forment-Allaga, P. Amoros, J. Ramirez-Castellanos and J. M. Gonzalez-Calbet, *J. Mater. Chem*., 2003, **13**, 3089; (*e*) M. Cavallini, F. Biscarini, J. Gomez-Segura, D. Ruiz and J. Veciana, *Nano Lett*., 2003, **3**, 1527; (*f*) A. Cornia, A. C. Fabretti, M. Pacchioni, L. Zobbi, D. Bonacchi, A. Caneschi, D. Gatteschi, R. Biagi, U. Del Pennino, V. De Renzi, L. Gurevich and H. S. J. Van der Zant, *Angew. Chem., Int. Ed*., 2003, **42**, 1645; (*g*) M. Clemente-Léon, H. Soyer, E. Coronado, C. Mingotaud, C. J. Gomez-Garcia and P. Delhaès, *Angew. Chem., Int. Ed*., 1998, **37**, 2842; (*h*) S. Willemin, B. Donnadieu, L. Lecren, B. Henner, R. Clérac, C. Guérin, A. Meyer, A. V. Pokrovskii and J. Larionova, *New J. Chem*., 2004, **28**, 919.

5 (*a*) C. Mingotaud, C. Lafuente, J. Amiell and P. Delhaes, *Langmuir*, 1999, **15**, 289; (*b*) J. T. Culp, J.-H. Park, D. Stratakis, M. W. Meisel and D. R. Talham, *J. Am. Chem. Soc*., 2002, **124**, 10083; (*c*) J. T. Culp, J.-H. Park, I. O. Benitez, Y.-D. Huh, M. W. Meisel and D. R. Talham, *Chem. Mater*., 2003, **15**, 3431.

6 (*a*) O. Hatlevik, W. E. Buschmann, J. Zhang, J. L. Manson and J. S. Miller, *Adv. Mater*., 1999, **11**, 914; (*b*) S. M. Holmes and G. S. Girolami, *J. Am. Chem. Soc*., 1999, **121**, 5593; (*c*) B. G. Morin, C. Hahm, A. J. Epstein and J. S. Miller, *J. Appl. Phys*., 1994, **75**, 5782; (*d*) J. S. Miller, *Adv. Mater*., 1994, **6**, 322; (*e*) S. Ferlay, T. Mallah, R. Ouahès, P. Veillet and M. Verdaguer, *Inorg. Chem*., 1999, **38**, 229; (*f*) W. E. Buschmann, S. C. Paulson, C. M. Wynn, M. Girtu, A. J. Epstein, H. S. White and J. S. Miller, *Adv. Mater*., 1997, **9**, 645; (*g*) W. R. Entley and G. S. Girolami, *Science*, 1995, **268**, 397; (*h*) S. Ferlay, T. Mallah, R. Ouahès, P. Veillet and M. Verdaguer, *Nature (London)*, 1995, **378**, 701; (*i*) V. Gadet, T. Mallah, I. Castro and M. Verdaguer, *J. Am. Chem. Soc*., 1992, **114**, 9213; (*j*) T. Mallah, S. Thiébaut, M. Verdaguer and P. Veillet, *Science*, 1993, **262**, 1554; (*k*) O. Sato, T. Iyoda, A. Fujishima and K. Hashimoto, *Science*, 1996, **271**, 49; (*l*) S. Ohkoshi and K. Hashimoto, *J. Am. Chem. Soc*., 1999, **121**, 10591.

7 (*a*) S. Vaucher, M. Li and S. Mann, *Angew. Chem., Int. Ed*., 2000, **39**, 1793; (*b*) S. Vaucher, J. Fielden, M. Li, E. Dujardin and S. Mann, *Nano Lett*., 2002, **2**, 225.

8 (*a*) T. Uemura and S. Kitagawa, *J. Am. Chem. Soc*., 2003, **125**, 7814; (*b*) D. M. DeLongchamp and P. T. Hammond, *Adv. Funct. Mater*., 2004, **14**, 224; (*c*) L. Catala, T. Gacoin, J.-P. Boilot, E. Rivier, C. Paulsen, E. Lhotel and T. Mallah, *Adv. Mater*., 2003, **15**, 826.

9 (*a*) P. Zhou, D. Xue, H. Luo and X. Chen, *Nano Lett*., 2002, **2**, 845; (*b*) J. G. Moore, E. J. Lochner, C. Ramsey, N. S. Dalal and A. E. Stiegman, *Angew. Chem., Int. Ed*., 2003, **42**, 2741.

10 J. M. Domingez-Vera and E. Colacio, *Inorg. Chem*., 2003, **42**, 6983.

11 (*a*) D. Zhao, J. Feng, Q. Huo, N. Melosh, G. H. Fredrickson, B. F. Chmelka and G. D. Stucky, *Science*, 1998, **279**, 548; (*b*) D. Zhao, Q. Huo, J. Feng, B. F. Chmelka and G. D. Stucky, *J. Am. Chem. Soc*., 1998, **120**, 6024.

12 (*a*) L. Mercier and T. J. Pinnavaia, *Adv. Mater*., 1997, **9**, 500; (*b*) A. Cauvel, G. Renard and D. Brunel, *J. Org. Chem*., 1997, **62**, 749;

(*c*) A. M. Liu, K. Hidajat, S. Kawi and D. Y. Zhao, *Chem. Commun*., 2000, **13**, 1145; (*d*) R. J. P. Corriu, E. Lancelle-Beltran, A. Mehdi, C. Reye, S. Brandes and R. Guilard, *J. Mater. Chem*., 2002, **12**, 1355.
13 P. K. Mascharah, *Inorg. Chem*., 1986, **25**, 15.
14 B. J. Corden, J. A. Cunningham and R. Eisenberg, *Inorg. Chem*., 1970, **9**, 357.
15 F. Bonadio, M. Gross, H. Stoekli-Evans and S. Decurtins, *Inorg. Chem*., 2002, **5**, 543.
16 K. Nakamoto, *Infrared and Raman Spectra*, John Wiley and Sons Inc., New York, 1986.
17 R. Köhn and M. Fröba, *Catal. Today*, 2001, **68**, 227.
18 (*a*) W. Hammond, E. Prouzet, S. D. Mahanti and T. Pinnavaia, *Microporous Mesoporous Mater*., 1999, **27**, 19; (*b*) M. Froba, R. Köhn and G. Bouffaud, *Chem. Mater*., 1999, **11**, 2858; (*c*) F. J. Brieler, M. Fröba, L. Chen, P. J. Klar and W. Heimbrodt, *Chem.-Eur. J*., 2002, **8**, 185; (*d*) F. J. Brieler, P. Grundmann, M. Fröba, L. Chen, P. J. Klar, W. Heimbrodt, H.-A. K. von Nidda, T. Kurz and A. Loidl, *J. Am. Chem. Soc*., 2004, **126**, 797.
19 *Theory and Applications of Molecular Paramagnetism*, eds. E. A. L. Boudreaux and N. Mulay, John Wiley Sons, New York, 1976.